Advanced Gas-cooled Reactors Technology for Enabling Molten-Salt Reactors Design - Optimisation of a New System.

Marat Margulis[a,b], Eugene Shwageraus[b,*]

[a] *Nuclear Futures Institute, School of Computer Science and Electronic Engineering, Bangor University, Bangor, LL57 2DG, United Kingdom*
[b] *Department of Engineering, University of Cambridge, CB2 1PZ, United Kingdom*

Abstract

Molten salts present significant advantages as coolants over traditional light water or gas. Salt-cooled nuclear reactor can potentially i allow an increase in core power density and simplify the reactor safety case. Traditionally, molten salt reactors assume molten salt being both the fuel and the coolant. This, however, creates major challenges for the design and operation due to requirements for chemistry control and corrosion behaviour of the core structural materials. The Fluoride salt-cooled High-temperature Reactors (FHR) on the other hand, have conventional solid fuel geometry surrounded by moderator and coolant. Furthermore, some FHR variations share many common characteristics with the Advanced Gas-cooled Reactors (AGR). Thus, using the knowledge accumulated during many decades of successful AGR operation can speed up the FHR development and deployment. However, replacing carbon-dioxide coolant by molten salt significantly changes the reactor performance. Hence, a new core design is needed. In this work, a Multi-Objective Particle Swarm Optimisation is used to identify the most favourable configurations for a new system layout. Initially, the optimisation targeted the beginning of cycle parameters such as criticality and Coolant Temperature Coefficient (CTC). The present work is the next step in this analysis. Each configuration is examined with respect to its thermal-hydraulic performance to assess the power uprate potential which is limited by multiple temperature constraints (e.g. fuel centreline and cladding temperatures as well as the coolant freezing/boiling). The estimated maximum power was then used in the fuel burnup calculations, from which a discharge burnup and cycle average CTC were obtained. As a result of the optimisation process, several families of possible solutions were identified, which form an optimal Pareto front. The most attractive configurations in terms of achievable power density, however, were not necessarily on the Pareto front. Most of the identified design options had only a small amount of graphite moderator or no graphite at all, relying entirely on moderation in the salt. Increasing the graphite volume was consistently found to worsen most of the optimisation parameters. The newly identified design options have the potential to achieve power density which is higher than that of a typical AGR by up to a factor of five, while maintaining negative CTC through the burnup cycle.

Keywords: AGR, FHR, AGRESR, MOPSO
Preprint submitted to Nuclear Engineering and Design *November 3, 2021*

*Marat Margulis
Email address: m.margulis@bangor.ac.uk (Eugene Shwageraus)

Abbreviation

AGR Advanced Gas-cooled Reactor.

AGRESR AGR Technologies for Enabling Molten Salt-cooled Reactor Design.

CTC Coolant Temperature Coefficient.

FHR Fluoride-salt-cooled High-temperature Reactors.

FLiBe Lithium Fluoride and Beryllium Fluoride.

MAGNOX MAGnesium Non-OXidising fuel reactor.

MOPSO Multi-Objective Particle Swarm Optimisation.

MSR Molten Salt Reactor.

PSO Particle Swarm Optimisation.

PWR Pressurised Water Reactor.

RBMK Reaktor Bolshoy Moshchnosti Kanalnyy (Large Power Channel Reactor).

UK United Kingdom.

WIMS Winfrith Improved Multi-group Scheme.

1. Introduction

Fluoride salt-cooled Hight-temperature Reactors (FHR) are a class of advanced reactors that combine many attractive features from the previous generation of nuclear power plants [1–3]. The FHR, unlike traditional molten-salt reactor (MSR) employs conventional solid fuel surrounded by graphite moderator and coolant, flowing around fuel pins, plates, or pebbles. Many similarities can be noted with other graphite-moderated systems, such as the UK MAGnesium Non-OXidising fuel reactor (MAGNOX) [4], and Advanced Gas-cooled Reactor (AGR) [5] both cooled by forced convection of CO_2 and the Soviet Union High-Power Channel-type Reactor (RBMK) [6], which is cooled by boiling water. Replacing traditional coolants (i.e., water or gas) by molten salt can potentially improve safety (by removing the requirement for the reactor

coolant circuit to be pressurised and allowing slower thermal transients) and increase power output (due to superior heat removal capabilities of molten salts) of the graphite-moderated reactor.

Among the mentioned reactor designs, the AGR have multiple common characteristics with some of the proposed FHR designs. The graphite-moderated core (geometry and structure), operating temperature range, neutron flux spectrum, pin-type fuel assembly are all relevant to the development of the FHR. However, it was demonstrated that direct replacement of gas coolant with salt has significant impact on the system performance, including safety characteristics [7]. Therefore, new systems require additional optimisation. This work reports on the results of such AGR-like FHR assembly-level optimisation.

The core characteristics chosen as performance parameters for comparison and optimisation were power density – as an indicator for capital costs and overall plant economics, and the ratio of discharge fuel burnup to initial fuel enrichment – as an indicator of fuel cycle cost. The optimisation was performed subject to a number of neutronic and thermal-hydraulic constraints. The coolant salt temperature coefficient of reactivity (CTC) was required to be negative on average during the fuel assembly irradiation. In principle, the most negative CTC is not necessarily the most attractive option. It can potentially be allowed to be positive as long as the whole system behaviour can be demonstrated to have favourable response to all limiting transient scenarios. Too negative CTC would also impose unnecessary economic penalty because the core heat-up reactivity decrement would need to be compensated by higher enrichment and would also result in greater reactivity control requirements to ensure shutdown margin. Nevertheless, in the absence of clear knowledge of AGR-like FHR transient behaviour, CTC was treated as an optimisation parameter rather than constraint.

Previous studies of AGR-like FHR [8, 9]] identified several possible design configurations. These studies were based on simplified but exhaustive search through the entire parametric design space searching separately for the best neutronic and thermal-hydraulic performance. As a result, two performance maps were obtained, one for neutronic and the other for thermal-hydraulic search spaces. Thus, to obtain a feasible solution, the two maps had to be superimposed.

This study is an extension of previous ones in several respects. It considers realistic fuel assembly geometry without making previously assumed simplifications such as modelling the fuel assembly as a representative fuel lattice unit cell with homogenised salt coolant and graphite moderator. Secondly, it models the fuel throughout its entire irradiation time, testing the cycle-average CTC rather the BOL one. Finally, it combines the neutronic and thermal-hydraulic search spaces, so that each configuration is tested against the constraints in both spaces. Due to the added complexity and computational costs of the new approach, the design optimisation process could no longer be done by exhaustive search. Instead, Multi-Objective Particle Swarm Optimisation algorithm (MOPSO) [10] was used in this study.

2. Methodology

In this study, the analyses were performed for configurations all of which share a number of common design features: pin-type fuel geometry, UO_2 fuel form in stainless steel cladding and lithium-beryllium fluoride (FLiBe) coolant salt. These choices arguably represent the least technological risks as substantial evidence and operational experience have been accumulated through their commercial use or R&D studies. More detailed description of the reference base-case fuel assembly designs is presented later in this section.

2.1. Computational Tools

2.1.1. WIMS Transport Code

The neutronic analyses were performed using deterministic neutron transport code WIMS - Winfrith Improved Multi-group Scheme [11]. It is a general-purpose fuel lattice code for 2D and 3D full core calculations. JEFF-3.1.2 based library [12] was used which has 172 energy groups. The code is capable of performing calculations for a wide range of nuclear systems using a diverse collection of deterministic transport solution methods. Using computationally efficient deterministic solvers in WIMS allowed reducing the calculation time for a single design evaluation in this work. This, in turn, enabled more rigorous and, therefore, reliable exploration of the design search space using the stochastic MOPSO algorithm in comparison to previous AGR-like FHR analysis [8, 9] where evaluations of the objective function were performed with a Monte Carlo code.

The AGR-like FHR design evaluations were performed using collision probabilities method. WIMS module PIJ calculates the first flight collision probabilities, whereas module PIP is used as the flux and eigenvalue problem solver using the collision probabilities calculated by PIJ. It should be noted that WIMS nuclear data library currently lacks temperature dependent cross section data for FLiBe isotopes. Therefore, the salt isotopes data was taken at the only available temperature of 300K, adding some uncertainty to the results. Therefore, the reactivity effect of the salt heat-up reported here is only due to thermal expansion of the salt. The following relationship for the salt density as a function of temperature was used [13]:

$$\rho(T) = 2.41303 - 4.884 \times 10^{-4} \cdot T \, [g/cm^3] \tag{1}$$

where T is in Kelvin.

2.1.2. Sub-Channel Thermal-hydraulic and Heat Transfer Solver - THERMO

Thermal-hydraulic calculations were performed using sub-channel code THERMO, which is a module in coupled code system BGCcore [14–16]. Given the assembly geometry, inlet flow rate, materials properties and power distribution, THERMO calculates the flow distribution between the coolant channels, core pressure drop as well as temperature fields in all of the core components. In this study, THERMO was used to identify

the maximum allowable power within a set of thermal-hydraulic constraints. These limits are summarised in Table 1. The analysis assumed that the tested assembly configuration is the hottest channel within the reactor core which has radial power peaking of 1.3. This maximum power peaking factor is representative of a typical AGR core [17]. Assuming that each of the considered fuel assembly design is loaded into position with the highest radial peaking factor allowed elimination of unsuitable configurations before the computationally expensive neutronic analysis is performed.

Axial power profile was obtained in earlier studies using coupled Serpent [18] and THERMO calculation for the reference AGR geometry [8]. This same axial power profile was assumed to be constant and used in all configurations studied in this work. Thermal properties of the salt coolant implemented in THERMO were taken from recent report in [13] and given by Eqs. (2) to (4) for the salt heat capacity, thermal conductivity and viscosity respectively.

Table 1: Thermal-hydraulic constraints of the AGR-like FHR model

Constraint	Value	Physical constraint
1. Max. fuel centreline temp.	2200 °C	UO_2 melting point at 2800 °C
2. Max. cladding temp.	1100 °C	Stainless steel melting point at 1400 °C
3. Max. coolant temp.	1100 °C	FLiBe boiling point at 1430 °C
4. Max. coolant bulk temp.	700 °C	Hastelloy N allows 730 °C
5. Min. coolant bulk temp.	470 °C	FLiBe freezing point at 450 °C
6. Max. pressure drop	350 [kPa]	Based on previous AGR-like FHR optimisation studies [19]
7. Min. local Reynolds	4000	Ensure turbulent flow for predictable heat transfer

$$C_p = 2385\,[J \cdot kg^{-1}K^{-1}] \tag{2}$$

$$k = 0.6297 + 0.0005 \cdot T\,[W \cdot m^{-1}K^{-1}] \tag{3}$$

$$\mu = 1.16 \times 10^{-4} \cdot e^{3755/T}\,[Pa \cdot s] \tag{4}$$

where T is in Kelvin.

2.2. Multi-Objective Particle Swarm Optimisation

The optimisation study in this work was performed using Particle Swarm Optimisation method (PSO)[20], which is a population-based meta-heuristic algorithm. The PSO algorithm is based on simulating the evolution of a swarm of particles, which explore an n-dimensional space in search of the best global solution. The position of each particle in the swarm is determined by evaluation of the objective function. The position is updated by adjusting the particle velocity, which is determined with respect to the personal and swarm

best known positions. The approach has been successfully applied to optimisation of non-linear and discrete single-objective problems.

The approach chosen in this study is to use traditional PSO to identify Pareto front of non-dominant solutions [21]. The historic record of best solutions found by a particle could be used to store non-dominant evaluation of the objective function generated in previous iterations. The use of global attraction mechanism combined with memory of previous solutions, i.e. previously found non-dominant population, would motivate the algorithm to converge towards Pareto front of non-dominant solutions. The MOPSO process is summarised in Algorithm 1, where the objective functions for this study are minimal fuel enrichment to burnup ratio (enrichment/BU) and minimal (negative) coolant temperature coefficient (due to the coolant thermal expansion effect only, as mentioned earlier).

Algorithm 1 MOPSO Algorithm

procedure MOPSO($n, constrains, maxIt$)
    Initialise the population POP and initial velocity:
    for i=0 to MAX **do** % MAX = number of particles
        Initialize POP(i)
        VEL(i) = 0
    Evaluate each of the particles if POP % run THERMO+WIMS
    Store the positions of the particles that represent non-dominant vectors in the repository REP Generate n-dimensional (nD) cubes of the search space explored, and locate the particles using the nD cubes as coordinate system where each particle's coordinates are defined according to the values of its objective functions.
    Initialise the memory of each particle
    for i=0 to MAX **do**
        PBEST(i) = pop(i)
    while $itr < maxIt$ **do** % maxIt = maximum number of iterations
        Compute the velocity, VEL(i), of each particle using expression in Eq. 5
        Compute new particle position POP(i) = POP(i) + VEL(i)
        Apply boundary condition of new particle positions
        Evaluate each particle in POP % run THERMO+WIMS
        Update the contents of REP together with the geographical representation of the particles within the nD cubes. This update consists of inserting all the non-dominant locations into the repository. Any dominant locations in the repository is eliminated.
        if current position is better than personal best **then**
            PBEST(i) = POP(i)
        itr = itr + 1
    Return $BestParticle$

Particle velocity is computed as follows:

$$VEL(i)_{t+1} = W \cdot VEL(i)_t + R_1 \cdot C_1 \cdot (PBEST(i) - POP(i)) + R_2 \cdot C_2 \cdot (REP(h) - POP(i)) \quad (5)$$

where W is the inertia weight, which helps to maintain the balance between exploration and exploitation

and was found to perform best when set to 0.4 [22]; R_1 and R_2 are random numbers sampled uniformly in the range $[0, 1]$; C_1 and C_2 are the personal and the global learning coefficients, both set to 2 [22]; $PBEST(i)$ is the best position that particle i remembers; $REP(h)$ is an objective function value taken from the repository; $POP(i)$ is the current objective function value of particle i. The selection of the index h is made as follows – the nD cubes containing more than a single particle are assigned a fitness equal to the result of dividing any number greater than 1 by the number of particles that they contain. Based on a sensitivity study, a value of 7 was selected. Any number above 7 gave similar result, but required longer simulation time. This aims to reduce the fitness of those nD cubes that contain large number of particles (i.e., fitness sharing [23]). Then, a roulette-wheel selection is applied to identify the nD cube from which the particle will be selected. Once the cube is selected, a particle from within it is obtained randomly. In the current analysis, 50 particles are sampled over 100 iterations, with a repository size of 50.

2.3. Discharge burnup estimation

The algorithm evaluates CTC through the burnup cycle by perturbing the salt density at each irradiation step. In order to obtain the enrichment-to-burn-up ratio, the discharge burn-up of each configuration must be estimated. Assuming an on-power or on-line refuelling, similar to that originally envisaged for an AGR. On-line refuelling, if implemented properly, can increase power plant availability. Unlike traditional batch fuel management in PWRs, which require complete shutdown of the plant for maintenance and refuelling, AGRs were designed to perform the refuelling while staying on-line (i.e. operating at full power), which would lead to longer periods between shutdowns needed only for maintenance. However, the operational experience was different, with only a few AGRs being able to perform the refuelling on-line, albeit at a reduced power. Nevertheless, the approach is very attractive for the future AGR-like FHR. To estimate the discharge burn-up in a on-line refuelling regime is twice of that of a single batch core. However, it is practically impossible to predict the shape of the reactivity curve (which can be either concave or convex) for different fuel compositions and salts. The linear reactivity model used to predict the discharge burn-up [24] for continuous online refuelling scheme can over- or under- estimate the actual discharge burn-up value. Therefore, the discharge burnup values are estimated as follows. For each configuration, the reactivity data is stored and fitted into a second order polynomial curve using Matlab fit function. For each curve, three first points are skipped to remove the influence of Xenon build-up. Then, second order derivative of the fitted polynomial is calculated. A positive value indicates that the reactivity curve is convex, while a negative value suggests a concave reactivity curve. Examples of typical concave and convex reactivity curves encountered in the study process are presented Fig. 1. As the design search space is unknown a priori, it was hard to foresee the exact shape of reactivity curves. Convex and concave shapes have been observed in preliminary studies as a result of different enrichment and moderation combinations. Figure 1 shows an exaggerated case for demonstration purposes only. The two curves shown also have different reactivity loss

rate with burnup and therefore each curve has different burnup axis with corresponding colour coding.

For conservatism, the discharge burn-up of assemblies with convex-shape reactivity curves are estimated as double that of a single-batch core. Configuration with concave-shape depletion curves, the fuel discharge burnup was estimated as the point at which the net excess of neutrons for the batch (integral of reactivity) over burnup for the studied configuration reaches zero. It should be noted that all neutronic simulations in the present work were performed in a 2D assembly model in WIMS. Thus, in order to account for leakage, a typical leakage reactivity worth, estimated for an AGR core, of 0.03 [17] was assumed in the discharge burn-up estimation [25].

Finally, fresh fuel enrichment has the strongest effect on the discharge burnup. Thus, for the same configuration and specific power, which is not a function of the fuel enrichment, the discharge burn-up may be different. Figure 2 shows reactivity curves of two hypothetical configurations. The two configuration layouts are identical, which means the maximum achievable power will be the same. However, the enrichment in configuration 1 is higher than in configuration 2. Thus, the discharge burn-up of configuration 1 will naturally be higher than for configuration 2.

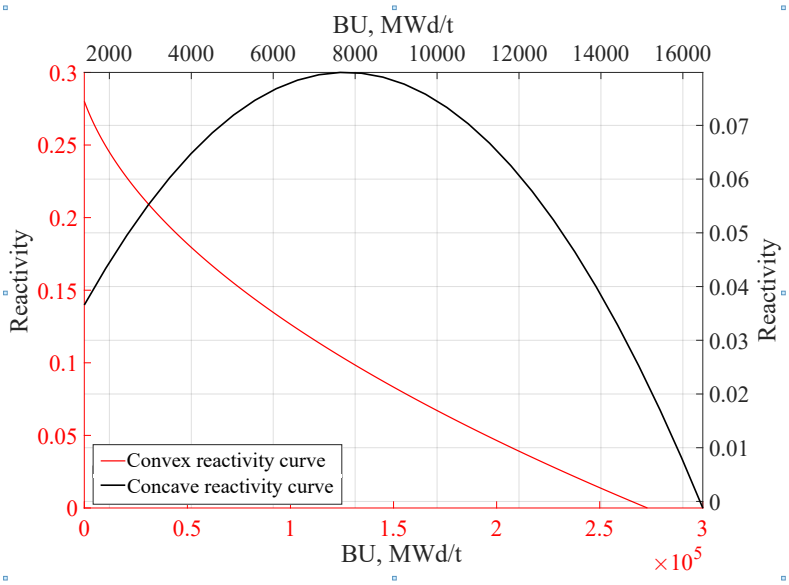

Figure 1: Example of reactivity curves observed in the optimisation process.

2.4. Reference AGR fuel assembly geometry

AGRs are using slightly enriched UO_2 fuel. The enrichment varies between approximately 1.16 and 2.1 w/o of ^{235}U. The fuel is encased in a stainless steel (type ATI 20-25+Nb) cladding and bound together in a graphite double sleeve (Fig. 3). The fuel element contains 36 fuel pins with a central tie-rod, which is used to connect up to 8 fuel elements into a stringer and pull the fuel assembly out of the core. The element dimensions are summarised in Table 2. The optimisation parameters and their boundaries are summarised

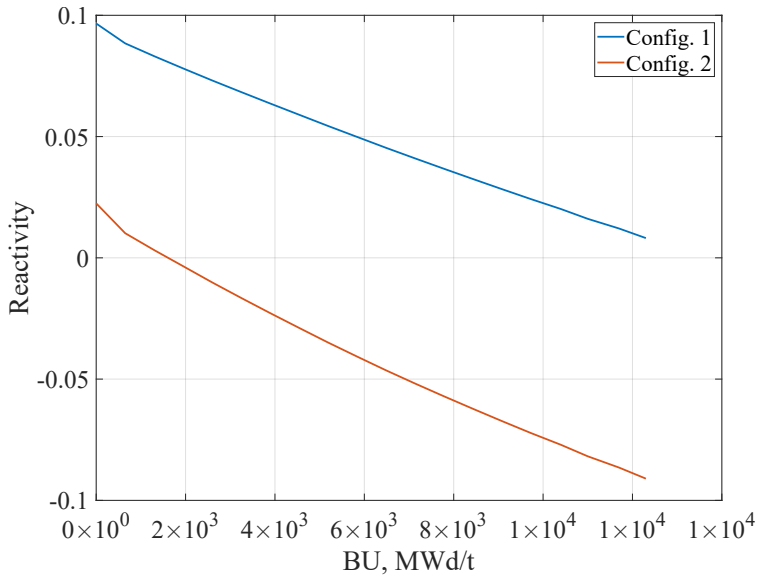

Figure 2: Reactivity curves example for same configuration with different enrichments.

in Table 3. The optimisation parameters bounds were selected based on the previous AGR-like FHR studies [19]. This includes the variation in such parameters as the number of pins in the inner ring and on diameter. The enrichment was varied from a typical AGR enrichment of about 1% to the maximum allowed under the non-proliferation restriction of 20%. Since, in some configurations, the graphite sleeve was removed completely, to compensate for reactivity loss, higher enrichment was required.

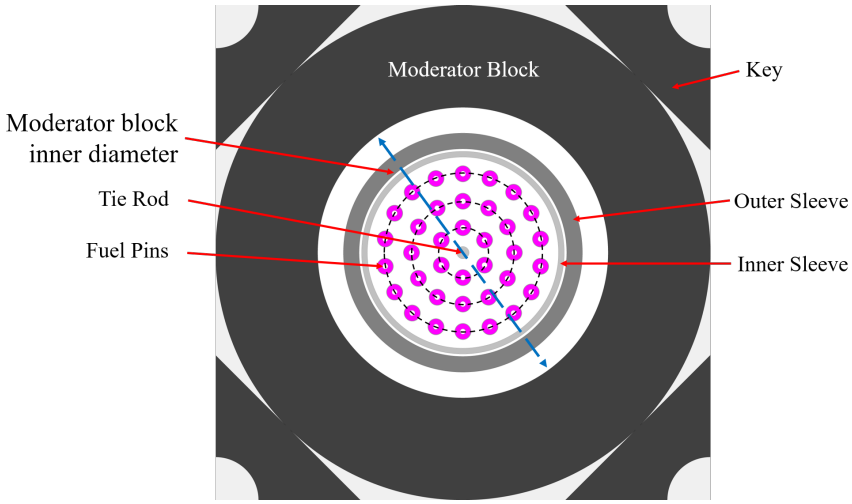

Figure 3: AGR reference fuel assembly layout.

The fuel assembly layout inside the moderator block is based on two parameters, the number of pins in the inner ring and the number of pins on the diameter. The reference geometry with inner block diameter d, pin radius r, has four pins in the inner ring, and eight pins on the diameter, as presented in Fig. 4a. The

Table 2: Main geometrical dimensions of AGR fuel element [5, 26].

Parameter	Value
Fuel pin outer diameter [mm]	14.5
Cladding thickness [mm]	0.38
Fuel length (1 section out of 8) [mm]	955
Radius of first (6) fuel pins ring [cm]	2.4
Radius of second (12) fuel pins ring [cm]	5.1
Radius of Third (18) fuel pins ring [cm]	7.6
Inner sleeve, inner diameter [cm]	19
Inner sleeve, outer diameter [cm]	22.2
Between sleeves gap thickness [mm]	2
Outer sleeve, inner diameter [cm]	22.6
Outer sleeve, outer diameter [cm]	23.8

Table 3: Optimisation parameters and their boundaries.

Optimisation Parameters	Value
Enrichment [w/o ^{235}U]	1 - 20
Fuel pin outer diameter [cm]	0.8 - 1.5
Moderator block inner radius [cm]	13.5, 17.5, 21.0
Pins in inner ring	4, 5, 6
Pins on diameter	8, 10, 12

total number of pins in an assembly can be manipulated by changing the number of pins in the inner ring, for example, as shown in Fig. 4b, where six pins are loaded in the inner ring. Thus, the number of pins in every consecutive ring is the multiplication of the ring index by the number of pins in the inner ring. The second option is changing the total number of pins in the assembly is changing the number of pins on the assembly diameter. For example, in Fig. 4c, the number of pins on the diameter was changed from eight to ten. Thus, relative to the reference configuration, there are five instead of four fuel rings. Finally, the combination of the two approaches is shown in Fig. 4d.

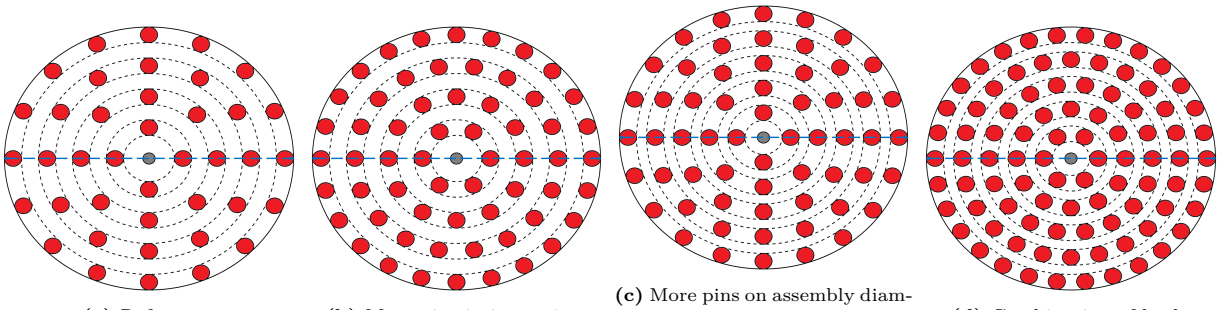

(a) Reference. **(b)** More pins in inner ring. **(c)** More pins on assembly diameter. **(d)** Combination of both.

Figure 4: Fuel assembly loading pattern example.

3. Results

The results of this study are presented in two parts. The first part examines the AGR-type fuel assembly and AGR-size core geometry as a reference. As mentioned earlier, previous studies have already suggested that substantial power uprate is possible by switching to molten-salt coolant in AGR-type geometries. As a result, the total power output of an AGR-size reactor would be unreasonably large to handle. Therefore, instead, the second part presents the results of optimisation study in which the core dimensions and number of fuel assemblies is similar to that of a typical Pressurised Water Reactor (PWR). The volume of such PWR-size core is about 5.3 times smaller than that of the AGR-size core (Table 4). This changes some of the assumptions regarding the core size and has effects on both neutronics as well as thermal hydraulics.

Table 4: Dimensions for system optimisation.

System	AGR-size	PWR-size
Fuel assembly height $[cm]$	830	360
Number of assemblies	332	144

3.1. AGR-size FHR

The results of the first part of the analysis are summarised in Fig. 5. The results along the Pareto front are marked by the red line. The figure shows a decrease in CTC with increasing enrichment to burnup ratio at low e/BU values. The CTC becomes negative at e/BU of about 2×10^{-5}. It indicates that there is a clear trade-off between the two objectives. On the other hand, at high enrichment to burnup ratios, the CTC settles on a relatively constant negative value.

The obtained results show some clustering of the solutions into families according to the moderator block sizes (Fig. 5). The block size effect on the results is significant. Configurations with the original block size (i.e., inner moderator block radius of 13.5 cm) with the largest amount of graphite among all of the considered cases achieve the best fuel cycle economics (lowest enrichment to burnup ratio). In contrast, configurations with the smallest amount of graphite (i.e., inner radius of moderator block radius of 21 cm) have the lowest CTC.

The power uprate potential is plotted in Fig. 6. The figure has the same coordinate axes, but the colour heat-map indicates a factor by which the core power can be increased relative to the reference CO_2-cooled AGR. The results suggest that the highest power uprate can be achieved for smaller graphite block sizes. Since power uprate was not one of the optimisation objectives, the highest power uprate case is not necessarily located on the Pareto front, as is the case here. Thus, based on the trade-off between different parameters (CTC, e/BU and power uprate), an AGR-like FHR of an AGR-size should contain much smaller quantity of graphite moderator than the reference AGR core (i.e., 50% or less).

In configurations with the original block size, salt mainly acts as a parasitic absorber. Therefore, thermal expansion of the salt leads to an increase in the number of neutrons that reach graphite block, slow down and return to the fuel. This appears to be the reason for strong positive reactivity feedback for cases with large graphite volume fraction (Fig. 5). On the other hand, for configurations with smaller graphite blocks, the salt acts as both, the coolant and moderator. Thus, changes in the salt density reduces the moderation and core reactivity. This tendency to achieve more favourable performance with diminishing amount of graphite suggests a realistic possibility of FHR core design with no graphite moderator block at all. Such configuration would resemble a PWR-like core rather than AGR-like one. This is a very significant and important finding of this study because the graphite core structure is the life limiting component of AGRs and its structural integrity behaviour with irradiation is a central part of AGR safety case. Removing this limitation would further promote the attractiveness of FHR with solid pin-type fuel.

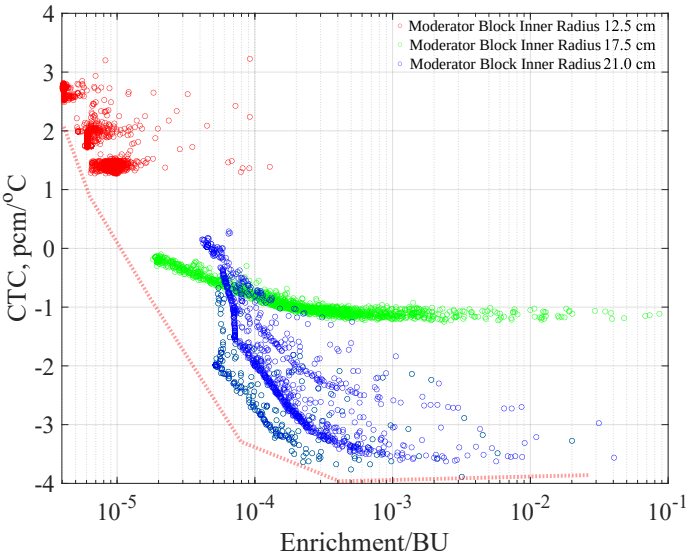

Figure 5: AGR scale FHR optimisation results.

The relationship between different optimisation parameters (enrichment, pin radius, moderator block inner radius, pins on diameter and inner ring) and primary (e/BU, CTC) and secondary (power density) objectives is visualised in a correlation matrix, shown in Fig. 7. The three parameters of interest are marked in yellow (power uprate, enrichment to burnup ratio and CTC). The effect of each design parameter on the optimisation objectives is not straightforward.

- Enrichment and CTC seem to have the strongest and positive correlation. An increase in enrichment leads to an increase in the magnitude of CTC. As can be seen from the results, the positive value of CTC becomes lower and eventually negative as the enrichment and moderator block size become smaller. In addition, a reduction in enrichment leads to lower enrichment to BU ratio.

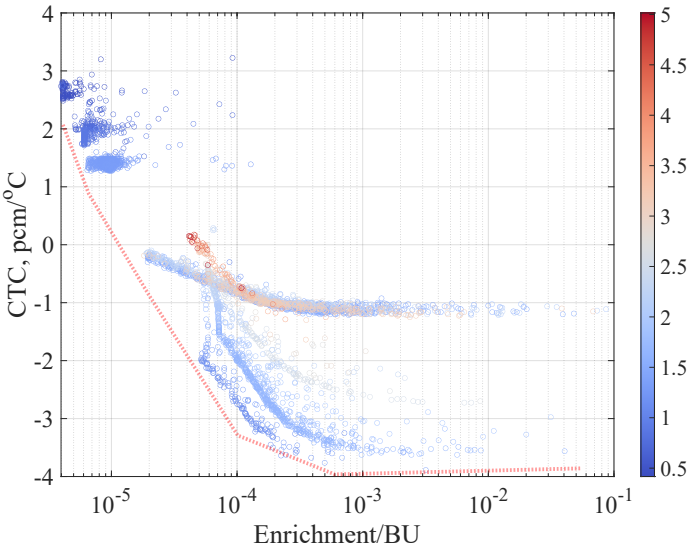

Figure 6: Power density uprate potential of AGR-size FHR.

- Moderator block inner radius strongly affects the optimisation objectives (e/BU, CTC, power density). As the graphite block size reduces, the CTC becomes more negative, thus, the negative correlation as noted previously. It also positively affects the power uprate potential as larger coolant flow area becomes available, also allowing an increase in the number of pins. However, an increase in power leads to shorter cycle (or more frequent refuelling rate for on-power refuelling as practised in some AGRs), as fissile material is depleted faster.

- Number of pins on the diameter has similar impact on the optimisation objectives as the fuel zone radius. Increase in the number of pins allows increasing power density, as there are more pins to bear the load, therefore, lower linear heat generation rate.

- The number of pins in the inner ring controls how dense the fuel pins in an assembly will be. Its only significant impact is on the power uprate because more pins per assembly allows to reduce the linear power rating and, thus, fuel temperature which typically limits the power density.

All the optimisation variables have fairly strong correlation with the optimisation objectives (0.4-1.0), except the number of pins on the diameter. The number of pins on the inner ring affects the number of pins in each subsequent concentric ring (multiplied by the ring index, Figs. 4a and 4b), which is relatively insensitive to the optimisation objectives (e/BU and CTC) as it does not affect much the amount of salt in the assembly, which , as can be seen from the correlation matrix, has a strong effect on the to CTC and e/BU.

The relationships described above can be also examined through observing the trade-off between enrichment and burnup which is plotted in Fig. 8. First, as expected, the discharge burnup shortens with

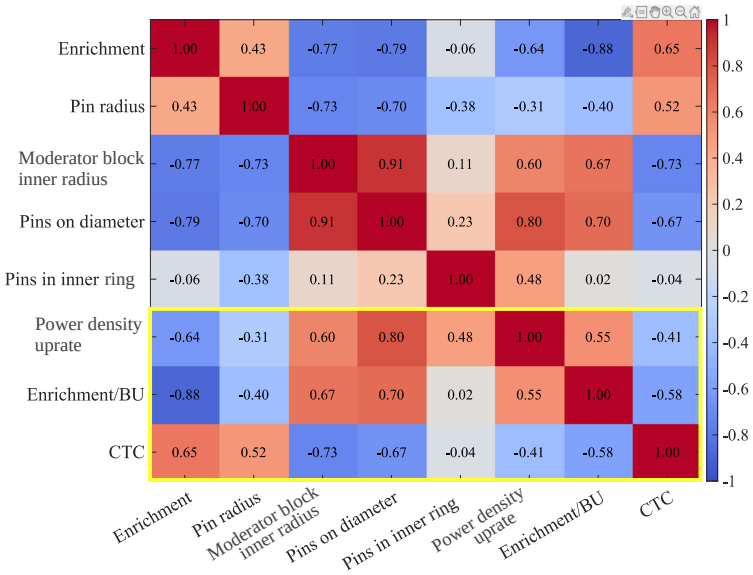

Figure 7: AGR scale FHR optimisation parameters correlation matrix.

decreasing enrichment (Fig. 8a). Furthermore, larger fuel zone radius (smaller moderator block) contributes to a decrease in achievable burnup despite an increase in enrichment, as can be seen in Fig. 8a. In addition, an increase in the number of fuel pins (Fig. 8b) also has negative effect on burnup.

Considering the relationship between enrichment, discharge burnup, geometry and CTC (Fig. 8c) it can be seen that as the fuel zone becomes smaller (or the graphite zone larger), the CTC becomes less negative and even positive. This trend occurs because the salt acts less as a moderator and more as a parasitic absorber in the smaller fuel zone configurations. In addition, CTC becomes more negative as the number of pins increases and the graphite block becomes smaller, as can be seen from Figs. 8b and 8c. Thus, the results suggest that the most favourable designs should have high enrichment (close to 20%), maximise the number of pins to ensure high discharge burnup and high power density, as well as negative CTC.

Finally, the optimisation results (Fig. 6) suggest that the highest power density uprate is achieved in configurations that are somewhat off the CTC versus e/BU Pareto front. The maximum power density uprate can be achieved for designs with the highest number of pins per assembly (about 70 fuel pins) and the smallest moderator block. However, for configurations with favourably low e/BU, the CTC becomes positive. Thus, a certain compromise on enrichment or fuel cycle economics is necessary to obtain a design with high power and comfortably negative CTC. Furthermore, lower enrichment will also contribute to the more negative fuel temperature coefficient.

3.2. PWR-size FHR

The MOPSO results for the smaller core case do not appear to be substantially different from the AGR-size case, as can be seen in Fig. 9. As in the AGR-size optimisation, the CTC becomes less negative as

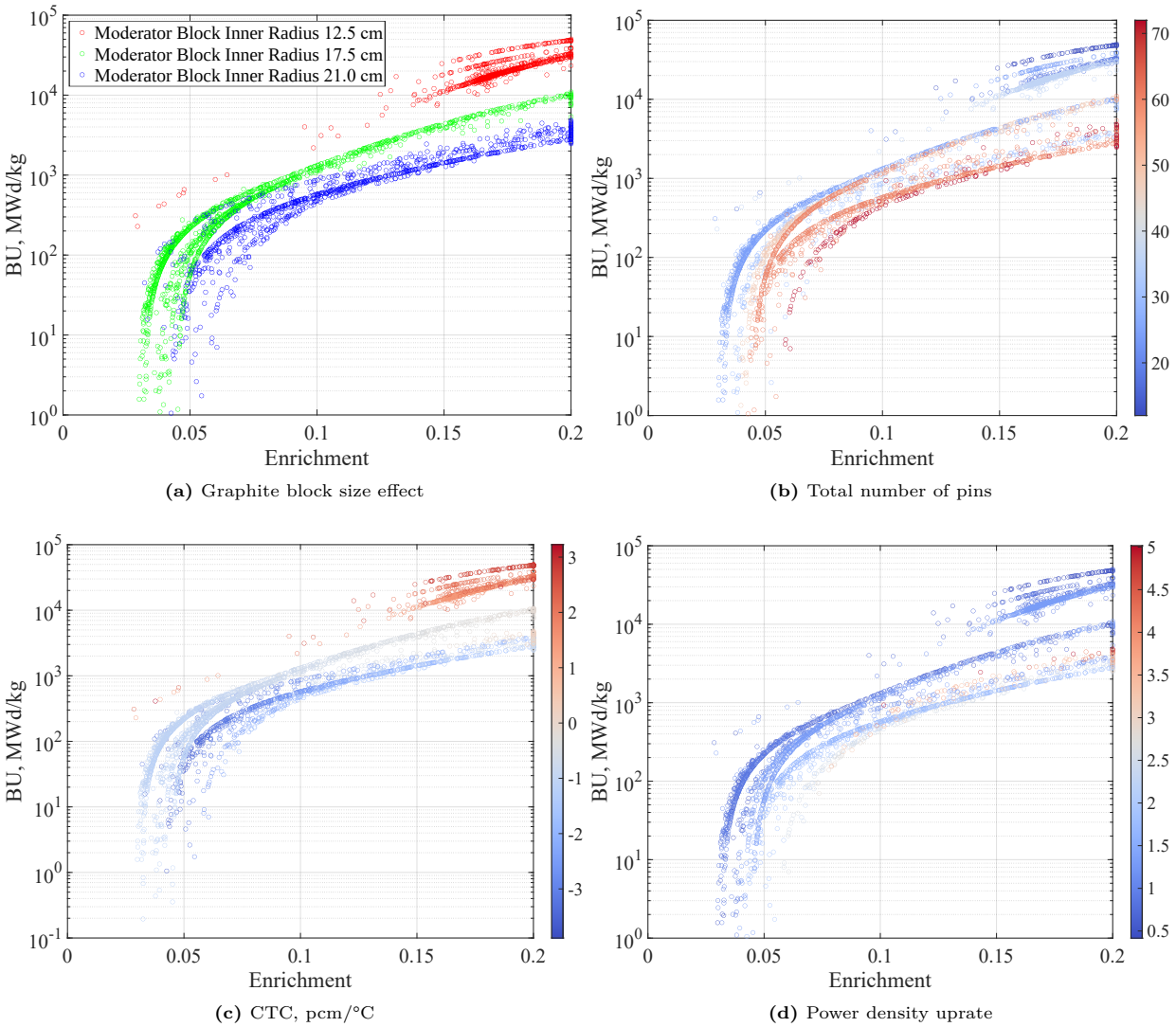

(a) Graphite block size effect

(b) Total number of pins

(c) CTC, pcm/°C

(d) Power density uprate

Figure 8: Enrichment vs. BU breakdown for selected parameters.

e/BU decreases and flattens as e/BU becomes larger. These results are encouraging and suggest that the AGR-like FHR can be scaled up and down in total power output or size without significantly affecting the choice of fuel assembly design parameters.

In both cases, the highest power density configuration resembles a light water-cooled system (almost no radial moderator, Fig. 11). Thus, after considering the trade-off between the optimisation parameters (CTC and e/BU) and power density uprate, the selected optimal configuration has power density uprate factor of about 5 times that of a typical AGR, while maintaining negative CTC through the burnup cycle. The thermal-hydraulic analysis of the hot channel of the optimised core is shown in Fig. 12. The limiting parameter is the fuel centreline temperature, as seen in Fig. 12 (fuel centreline approaches the 2200°C limit). The rest of the temperatures do not breach the adopted constraints (Table 1). As the fuel pin becomes larger

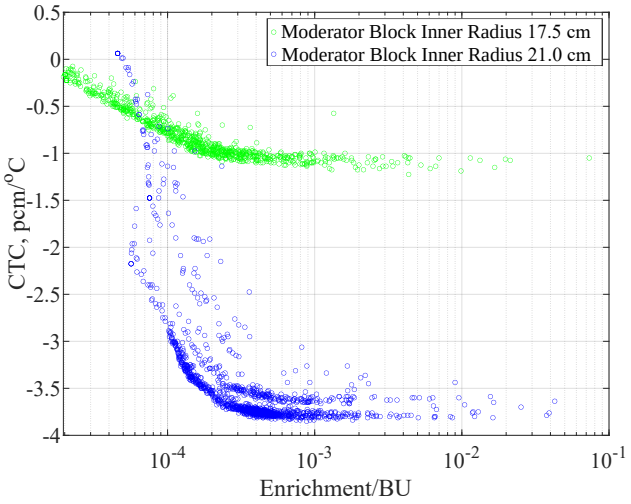

Figure 9: PWR scale FHR optimisation results.

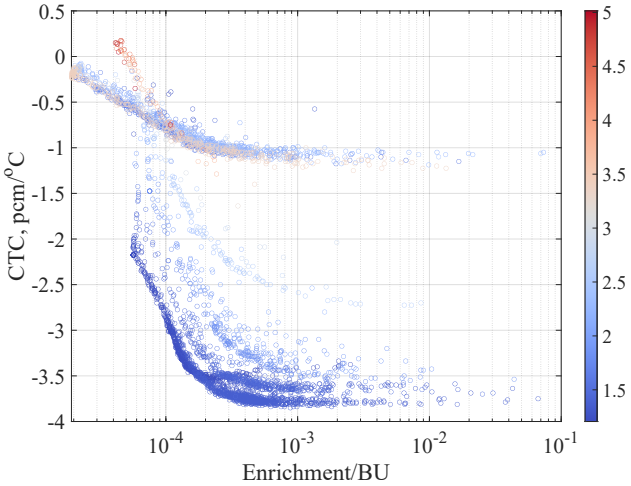

Figure 10: PWR scale FHR optimisation results as function of power.

(radius 1.443 cm in the optimised model versus 0.7663 in the reference AGR) the heat conduction through the pin becomes the dominant thermal resistance in the overall heat transfer mechanism. Thus, for a given assembly power, there would be fewer larger-diameter pins and, therefore, linear power will increase leading to higher centreline temperature. Coolant temperature rise across the core is small, as shown in Fig. 12. It should be noted that among all the examined configuration (150,000+ simulations) the limiting thermal-hydraulic parameter was the fuel centreline temperature and the pressure drop across the core. Cladding temperature constraint, salt boiling and freezing limits were never the most limiting.

Previous studies found similar relationship between CTC and e/BU [27]. However, they did not conclusively show what the trade-offs are with achievable power uprate or geometry. The current analysis demonstrates the relationship between different design variables affecting the design objectives of a new

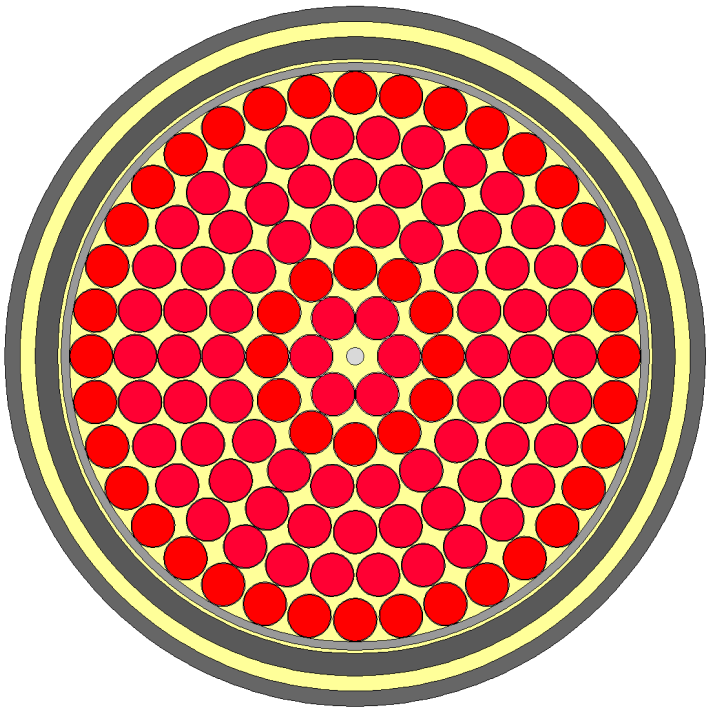

Figure 11: Optimised geometry (Gray - graphite sleeve and 1 cm thick block for channel isolation.

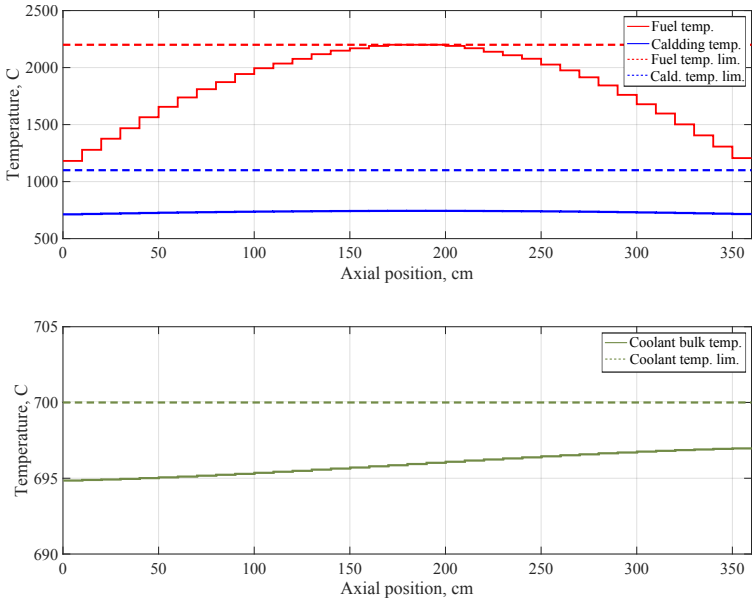

Figure 12: Optimised geometry thermal-hydraulic analysis results.

system. As mentioned, the optimisation objectives trends generally agree with those observed in the previous studies. This study, however, identified the most attractive configurations with respect to the three design objectives simultaneously: fuel cycle cost (enrichment/burnup), safety (CTC) and capital cost (power

density uprate). A map of 3-dimensional Pareto front (surface) generated in this study shows useful relationships between the different design parameters and can be used as a guideline for new, more detailed core design studies.

The selected most attractive configuration presented above is based not solely on the optimisation results, but also on expert judgement of the designers (i.e., including power density uprate factor in the selection of optimal configuration). Table 5 shows comparison between the two cases taken from the Pareto front (Cases 1 and 2) and the case presented earlier in the text (Case 3). As mentioned previously, the configurations located on the Pareto front are not necessarily the ones with the highest power uprate factor. The highest power uprate cases are located away from the Pareto front (Figs. 6 and 10). The evolution of the infinite multiplication factor and CTC as a function of BU for these cases are summarised in Fig. 13. It can be seen, that Cases 1 and 2 have very similar starting point, but their burnup curves evolve differently, as their heavy metal content is different. The three presented cases achieve higher discharge burnup in comparison to typical AGR, which is about 18 MWd/kg [5]. The CTC in all cases remains negative on average through the cycle, but as can be seen in Fig. 13b, it changes sign in Case 3, starting from about -1 pcm/°C and reaching about 0.25 pcm/°C at discharge. In Cases 1 and 2, on the other hand, the CTC value always remains negative. Please note that WIMS prints out the reactivity variation rounded off to an integer number of pcm's. As a result, the curves of CTC versus burnup exhibit some discontinuous behaviour.

The results presented in Table 5 verify the findings of the optimisation algorithm and suggest that considering Case 3 as optimal is appropriate. Although, Cases 1 or 2 benefit from higher BU, it is beyond the current operational experience, therefore, casting doubt on whether such high values can be considered realistic. On the other hand, burnup in Case 3 is within the current PWR experience, reducing the technological uncertainty of the new fuel design. Thus, Case 3 can be considered a feasible example of optimal fuel design for future, more detailed, development of a graphite-free FHR concept.

Table 5: Different case data comparison.

Case	Block rad.,[a] cm	# pins	Pin diam., cm	e	BU, MWd/kg	CTC[b]	Power density uprate
1	17.5	60	1.38	20%	233	-0.2	3.1
2	21	30	0.80	20%	170	-2.2	1.1
3[c]	21	72	1.44	10.15%	64	-0.1	5.0

[a] Moderator block inner radius.
[b] Average value through the cycle, pcm/°C.
[c] Designers' judgement included.

4. Conclusions

This paper presents core design optimisation results of a new FHR concept based on AGR technology. Despite already substantial FHR R&D efforts, some parts of potential FHR design space remain largely un-

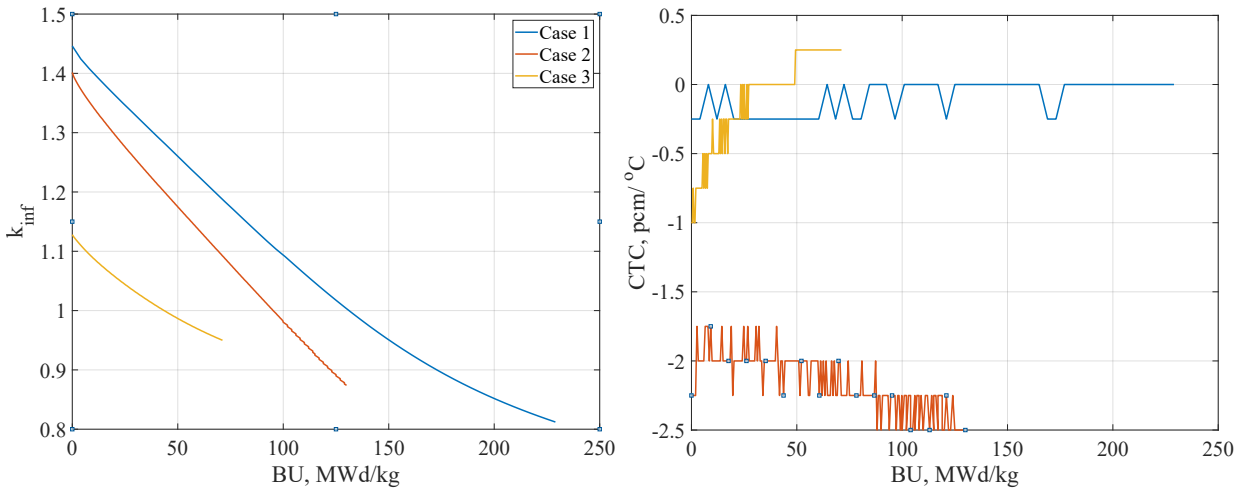

(a) Infinite multiplication factor **(b)** CTC

Figure 13: Variation of parameters of the different cases as function of burnup.

explored, and many studies are still ongoing. Taking advantage of the resemblance between FHRs and AGRs can reduce the time needed for development and commercialisation of FHRs. Although AGR development was a long and technically challenging process, all issues have eventually been resolved and well-understood by now. Such long process led to deployment of a unique reactor fleet with remarkable operating and safety record.

Utilising light-isotopes based salt such as FLiBe, which provide significant neutron moderation, along with separate solid graphite moderator make the system potentially less stable because of a possibility of positive reactivity feedback due to the coolant salt thermal expansion. This is undesirable from the safety and operational stability point of view and, therefore, to be avoided. Thus, in order to assure negative CTC and improve the reactor economics, a multi-objective optimisation is needed. The two optimisation parameters selected were the CTC and enrichment to burnup ratio. The MOPSO algorithm was chosen to perform the optimisation.

The design search space for the studied reactor concept is complex, as numerous design variables affect the optimisation objectives. In this study, the following design variables were considered - enrichment, pin radius, fuel zone radius, number of pins on diameter and in the inner ring. Thermal hydraulic performance of each configuration was evaluated using THERMO code to determine the maximum achievable power for that configuration. The obtained power could be constrained by one of the following thermal limits: fuel centre line temperature, cladding temperature, maximum/minimum coolant temperature, minimum Re number to ensure turbulent flow, and a given fixed pressure drop (selected based on previous studies). The obtained power is then used in neutronic burnup simulation using WIMS code to estimate the discharge burnup and obtain the enrichment to burnup ratio.

The optimisation results showed that there is a clear trade-off between the two optimisation objectives. In shorter fuel cycles, for high enrichment to burnup ratios, the CTC was found to be independent of the enrichment-to-burnup ratio and remained negative. As the enrichment to burnup ratio becomes smaller (indicating better fuel cycle economics), the CTC becomes less negative and eventually positive, restricting the possibility for achieving best possible fuel cycle cost. However, when introducing a third parameter of interest, namely, the core power density, the configurations located on the Pareto front were found to be less attractive. Designs with the most significant improvement in power density were found in the cloud of the optimisation results, indicating additional trade-off with this third objective.

The first part of the current optimisation study was performed on a system with the core size similar to a typical AGR. The second set of optimisations tested the impact of the core dimensions on the enrichment to burnup ratio and CTC design objectives. The alternative system size was chosen to be similar in height and number of fuel assemblies to a typical pressurised water reactor. The results showed that there is no significant difference in the shape and location of the Pareto front.

Taking into account configurations with the highest power density revealed that minimum amount of graphite was the common feature for all of these configurations, resembling more a light water reactor system rather than an AGR. The graphite block was practically eliminated in these cases, while only a thin assembly sleeve remained to ensure the channel separation. The number of pins was increased substantially, minimising the spacing between the pins. The increased number of fuel pins allowed increasing the linear heat generation rate, leading to higher achievable power density.

The optimisation design space explored in this study provides a view of a broad range of potential candidates for a design of an AGR-like FHR, conveniently showing the trade-offs between the safety parameters, fuel cycle economics and power uprate potential. The following step will be the design of a full core model based on the findings in this work. Furthermore, FLiBe coolant, even with isotropically enriched lithium, will inevitably produce some tritium which will need to be managed (removed and stored). This may or may not prove to be prohibitively technologically complex or costly challenge. Therefore, future analyses of alternative, non-tritium-producing salt coolants will be performed.

5. Acknowledgements

This work was partially supported by the UK Engineering and Physical Sciences Research Council under grant EP/R029113/1 – AGR Technology for Enabling Salt-cooled Reactor Designs (AGRESR).

References

1. Holcomb DE, Flanagna GF, Mays GT, Poiter DW, Robb KR, Yoder Jr. GL. Fluoride Salt-Cooled High-Temperature Reactor Technology Development and Demonstration Roadma. Tech. Rep. ORNL/TM-2013/401; ORNL; 2013.
2. Forsberg C, Peterson PF. Basis for Fluoride Salt–Cooled High-Temperature Reactors with Nuclear Air-Brayton Combined Cycles and Firebrick Resistance-Heated Energy Storage. *Nuclear Technology* 2017;196(1):13–33. doi:10.13182/NT16-28.
3. Forsberg C, Wang D, Shwageraus E, Mays B, Parks G, Coyle C, Liu M. Fluoride-salt-cooled high-temperature reactor(fhr) using british advanced gas-cooled reactor(agr) refueling technology and decay heat removal systems that prevent salt freezing. *Nuclear Technology* 2019;205(9):1127–42. doi:10.1080/00295450.2019.1586372.
4. Nonbol E, Jensen SE. Description of the Magnox Type of Gas Cooled Reactor (MAGNOX). Tech. Rep. NKS/RAK2(97)TR-C5; Riso National Laboratory; Roskilde, Denmark; 1998.
5. Nonbol E. Description of the Advanced Gas Cooled Type of Reactor (AGR). Tech. Rep. NKS/RAK2(96)TR-C2; Riso National Laboratory; Roskilde, Denmark; 1996.
6. Dollezhal, N A . Graphite-water steam-generating reactor in the USSR. *Nuclear Energy* 1981;20(5):385–90.
7. Margulis M, Shwageraus E. Advanced Gas-cooled reactors technology for enabling molten-salt reactors design - Estimation of coolant impact on neutronic performance. *International Journal of Energy Research* 2020;125:1–19. doi:10.1016/j.pnucene.2020.103382.
8. Xing Z, Shwageraus E. Design Space Exploration Studies of an FHR Concept Leveraging AGR Technologies. In: *In Proc. of ICAPP2017*. Fukui-Kyoto, Japan: ICAPP; 2017:.
9. Xing Z, Shwageraus E. Molten Salt Coolant Reactivity Fedback in Alternative FHR Designs. In: *In Proc. of PHYSOR2018*. Cancun, Mexico: American Nuclear Society; 2018:.
10. Coello CAC. An Introduction to Multi-Objective Particle Swarm Optimizers. In: Gaspar-Cunha A, Takahashi R, Schaefer G, Costa L, eds. *Soft Computing in Industrial Applications*. Berlin, Heidelberg: Springer Berlin Heidelberg. ISBN 978-3-642-20505-7; 2011:3–12.
11. Lindley BA, Hosking JG, Smith PJ, Powney DJ, Tolit BS, Newton TD, Perry R, Ware TC, Smith PN. Current status of the reactor physics code WIMS and recent developments. *Annals of Nuclear Energy* 2017;102:148–57. doi:https://doi.org/10.1016/j.anucene.2016.09.013.
12. Nuclear Energy Agency of the OECD . JEFF 3.1.2 - Joint evaluated nuclear data library for fission and fusion applications. DVD; 2012.
13. Romatoski RR, Hu LW. Fluoride salt coolant properties for nuclear reactor applications: A review. *Annals of Nuclear Energy* 2017;109:635 –47. doi:https://doi.org/10.1016/j.anucene.2017.05.036.
14. Kotlyar D, Shaposhnik Y, Fridman E, Shwageraus E. Coupled neutronic thermo-hydraulic analysis of full PWR core with Monte-Carlo based BGCore system. *Nuclear Engineering and Design* 2011;241(9):3777 –86. doi:https://doi.org/10.1016/j.nucengdes.2011.07.028.
15. Margulis M, Shwageraus E. Extending Two-Phase Capabilities of Thermal-Hydraulic Module in BGCore. In: *In Proc. of the 27th Conference of the Nuclear Societies in Israel*. Dead Sea, Israel: Israel Nuclear Society; 2014:.
16. Margulis M, Gilad E. Development and Verification of the Dynamic System Code THERMO-T for Research Reactor Accident Analysis. *Nuclear Technology* 2016;196(2):377–95. doi:http://doi.org/10.13182/NT16-23.
17. Nuwayhid RY. Assessment of thermal and fast reactor designs based upon the advanced gas-cooled reactor. Ph.D. thesis; University of London; 1989.
18. Leppänen J, Pusa M, Viitanen T, Valtavirta V, Kaltiaisenaho T. The Serpent Monte Carlo code: Status, development and applications in 2013. *Annals of Nuclear Energy* 2015;82:142 –50. doi:https://doi.org/10.1016/j.anucene.2014.08.024.
19. Xing Z. Design space exploration for salt cooled reactor systems. Ph.D. thesis; University of Cambridge; 2021.

20. Kennedy J, Eberhart R. Particle Swarm Optimization. In: *In Proc. of International Conference on Neural Networks - ICNN'95*. Perth, WA, Australia; 1995:.
21. Seah CW, Ong YS, Tsang IW, Jiang S. Pareto Rank Learning in Multi-objective Evolutionary Algorithms. In: *In IEEE Congress on Evolutionary Computation*. Brisbane, QLD, Australia; 2012:.
22. Dasheng L. Multi-objective particle swarm optimization: Algorithms and applications. Ph.D. thesis; Tianjin University; 2008.
23. Goldberg DE, Richardson J. Genetic algorithms with sharing for multimodal function optimization. In: *In Proc. of the Second International Conference on Genetic Algorithms on Genetic algorithms and their application*. Cambridge, Massachusetts, USA; 1987:.
24. Driscall MJ, Downar TJ, Pilat EE. The linear reactivity model for nuclear fuel management. La Grange Park, Ill., USA : American Nuclear Society; 1990.
25. Kotlyar D, Shwageraus E. Comparison of square and hexagonal fuel lattices for high conversion PWRs. *Kerntechnik* 2012;77(4):292–9.
26. VOLUME J - Nuclear Power Generation. In: *Modern Power Station Practice (Third Edition)*. British Electricity International; Oxford: Pergamon; third edition ed. ISBN 978-0-08-040735-7; 1992:260 –5. doi:https://doi.org/10.1016/B978-0-08-040735-7.50017-X.
27. Ingersoll DT. Status of Physics and Safety Analyses for the Liquid-Salt-Cooled Very High-Temperature Reactor (LS-VHTR). Tech. Rep. ORNL/TM-2005/218; ORNL; 2013.